Wireless Networks (2020) 26:5151–5162
https://doi.org/10.1007/s11276-020-02380-6

Optimal sensor placement for source localization based on RSSD

Ali Heydari[1] · MasoudReza Aghabozorgi[1] · Mehrzad Biguesh[2]

Published online: 12 June 2020
© Springer Science+Business Media, LLC, part of Springer Nature 2020

Abstract
Source localization based on the received signal strength (RSS) has received great interest due to its low cost and simple implementation. In this paper we consider the source localization problem based on the received signal strength difference (RSSD) with unknown transmitted power of the source using spatially separated sensors. It is well- known that the relative sensor-source geometry (SSG) plays a significant role in localization performance. For this issue, the fisher information matrix (FIM) which inherently is a function of relative SSG is derived. Then for different scenarios the SSG based on the maximization of determinant of FIM is investigated to obtain the optimal sensor placement. Finally, computer simulations are used to study the performance of various sensor placements. Both theoretical analysis and simulation results reveal the ability of the proposed sensor- source geometries.

Keywords Source localization · Optimal sensor placement · Fisher information matrix (FIM) · Cramer Rao bound (CRB) · Sensor-source geometry (SSG) · Received signal strength difference (RSSD)

1 Introduction

Source localization, has been attractive in many research fields such as wireless sensor networks (WSNs), mobile communication, microphone array, radio astronomy [1–13]. Several techniques are available for source localization, including time of arrival (TOA) [14, 15], time difference of arrival (TDOA) [10, 13], angle of arrival (AOA) [16, 17], received signal strength (RSS) [16, 18], frequency doppler, and combination of these techniques [7–9, 19, 20]. Among these methods, the TOA and TDOA based methods usually provide better results but they are expensive to implement [9]. On the other hand, the AOA based method, requires sensors with multiple antennas or rotating directional antenna to obtain the AOA of source [21]. In contrast, the energy based methods using the received signal strength (RSS) or the received signal strength differences (RSSD) are attractive due to their low cost and simple implementation [22–25]. Unlike the RSS-based localization, the RSSD based localization has not been adequately investigated. In RSSD method the difference of the powers measured by a pair of sensors, in a homogenous environment defines a circle where the source could lay on it. As a result, the source location is obtained using the intersection of at least two of such circles [25]. Since the signal power measurements are noisy, therefore instead of the single cross-point, we encounter with ambiguous areas. The source location estimation methods attempt to deal with these uncertainty areas in different ways. There are several well-known RSSD-based methods for estimating the location of source. A linear least squares (LLS) technique was developed by Liu in [22]. In [3], a minimax optimization and semidefinite programming was applied to estimate the source location which is efficient for large signal-to-noise ratio scenarios. Nonlinear least squares (NLS) method was developed in [25]. A weighted least squares (WLS) method using the unscented transformation (UT) was derived in [26]. An important issue that can severely affect the performance of any localization algorithm is the relative sensor-source geometry (SSG). In

✉ MasoudReza Aghabozorgi
aghabozorgi@yazd.ac.ir

Ali Heydari
heydari90@gmail.com

Mehrzad Biguesh
biguesh@shirazu.ac.ir

[1] Department of Electrical Engineering, Yazd University, Yazd, Iran

[2] Department of Electrical Engineering, Shiraz University, Shiraz, Iran

[27, 28], the conditions that lead to the optimal sensor geometry for AOA-localization was derived. In [29], the optimal geometries of a group of sensors for TDOA-based localization using both centralized and non-centralized method was addressed. Two-dimensional sensor placement using time difference of arrival measurements was studied in [30]. Optimal sensor arrangement based on RSS was also studied in [31]. There are also papers that have analyzed the optimal SSG in heterogeneous sensor networks [32]. For optimal sensor placement based on the TDOA, AOA and RSS measurements three optimality criteria are mainly considered in literature which includes maximization of determinant of fisher information matrix (FIM), maximization of the smallest eigenvalue of FIM, and minimization of the trace of the inverse of FIM. It is important that using any of these criteria lead to different result for optimal sensor placement. In this paper we study the optimal sensor-source geometry for RSSD based source localization. For this issue, at the first we derive the FIM matrix then we use the determinant of FIM as our desired criterion to obtain the optimal SSG. After that, we use this criteria in various scenarios and obtain the conditions which lead to the optimal SSG. The rest of this paper is organized as follows. In Sect. 2, we introduce our assumed system model and the required formulations for RSSD measurements. In Sect. 3, we derive the FIM for our localization problem. Based on the determinant of FIM, the optimal sensor placement is discussed in Sect. 4. Simulation results and analysis are provided in Sect. 5. Finally, Sect. 6 presents the conclusion of this study.

Throughout this paper, vectors and matrices are shown with bold lowercase and bold uppercase letters; respectively. $|\mathbf{A}|$ shows the determinant of matrix $\mathbf{A}$, $\|\cdot\|$ denotes the Euclidean norm, and $\|\mathbf{a}\|_{\mathbf{H}}^2 \triangleq \mathbf{a}^{\mathbf{T}}\mathbf{H}\mathbf{a}$. The (i, j)-th entry of matrix $\mathbf{A}$ is denoted by $[\mathbf{A}]_{i,j}$, $[\mathbf{a}]_i$ represents the ith element of vector $\mathbf{a}$, and superscript $\cdot^T$ denotes the transpose of a vector or a matrix. Finally, $E\{\cdot\}$ is used for the statistical mean of a random variable.

2 The RSSD signal model

We consider a stationary source with unknown location at $\mathbf{p} = [x\ y]^T \in \mathbb{R}^2$ and $N \geqslant 3$ sensors at known locations $\mathbf{s}_i = [x_i\ y_i]^T$ for $i = 1, 2, \ldots, N$. Our localization scenario is illustrated in Fig. 1.

The distance between the source and the ith sensor is $r_i = \|\mathbf{p} - \mathbf{s}_i\|$ and $\theta_i = \angle(\mathbf{p} - \mathbf{s}_i)$ is the bearing angle between the source and the ith sensor. The RSS at the ith sensor in the absence of noise whenever the environment is homogenous can be modeled as [33]

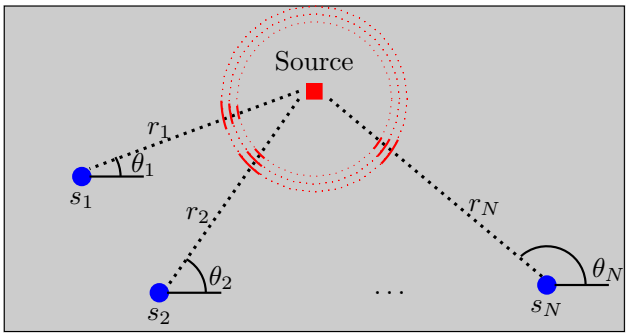

Fig. 1 An example of a system of sensors for finding the location transmitter in the region

$$P_i = K_0 \frac{P_t}{r_i^{\gamma}} \quad \text{for } i = 1, 2, \ldots, N \tag{1}$$

where P_t denotes the source transmit power, γ is the path loss exponent, and K_0 is the loss component that depends on the system factor. The path loss exponent γ is a function of the environment and can be a vlaue between 1 and 6 and we suppose that it is known in this work. Assuming a log-normal distribution for P_i, then its measured value in dB is [23]

$$\widetilde{P}_i = 10\log(K_0) + P_t - 10\gamma\log_{10} r_i + \varepsilon_i \quad \text{for } i = 1, \ldots, N. \tag{2}$$

Here, ε_i is the added term due to the noisy measurement which is assumed to be zero-mean Gaussian with variance σ_i^2, where $\mathrm{E}\{\varepsilon_i\varepsilon_j\} = 0$ for $i \neq j$. In our assumed system without loss of generality if we take the Nth sensor as the reference sensor, then the RSSD between the ith sensor and the reference sensor will be

$$\widetilde{\Delta}_i \triangleq \widetilde{P}_i - \widetilde{P}_N + n_i = 10\gamma\log_{10}\left(\frac{r_N}{r_i}\right) + n_i, \quad \text{for } i = 1, \ldots, N. \tag{3}$$

In the above relation, $n_i \triangleq \varepsilon_i - \varepsilon_N$ is the RSSD measurement noise which is the zero-mean Gaussian with variance $(\sigma_i^2 + \sigma_N^2)$.

Let us define

$$\Delta \triangleq \left[10\gamma\log_{10}\left(\frac{r_N}{r_1}\right) \quad \cdots \quad 10\gamma\log_{10}\left(\frac{r_N}{r_{N-1}}\right)\right]^T \tag{4}$$

$$\mathbf{n} \triangleq [n_1 \quad \cdots \quad n_{N-1}]^T \tag{5}$$

As a result, the RSSD measurement vector can be written in the following vector form

$$\widetilde{\Delta} = \begin{bmatrix} \widetilde{\Delta}_1 \\ \vdots \\ \widetilde{\Delta}_{N-1} \end{bmatrix} = \Delta + \mathbf{n}. \tag{6}$$

Since $E\{\varepsilon_i \varepsilon_j\} = 0$ for $i \neq j$ and using the following relation

$$E\{n_i n_j\} = E\{(\epsilon_i - \epsilon_N)(\epsilon_j - \epsilon_N)\} = \begin{cases} \sigma_i^2 + \sigma_N^2 & \text{for } i = j \\ \sigma_i^2 & \text{for } i \neq j \end{cases} \tag{7}$$

the covariance matrix of noise vector $\mathbf{n}$ can be obtained as

$$\boldsymbol{\Sigma} = E\{\mathbf{n}\mathbf{n}^T\} = \sigma_n^2 \mathbf{1} + \text{diag}(\sigma_1^2, \ldots, \sigma_{N-1}^2), \tag{8}$$

where $\mathbf{1}$is the $(N-1)$ square matrix with all entries one, and diag$(\cdot)$ represents the diagonalization operator.

3 FIM based on RSSD

In this section we derive the FIM matrix and Cramer-Rao bound (CRB) matrix for our localization problem. If $\mathbf{x}$ is an unknown vector to be estimated from the measurement $\widehat{\mathbf{z}} = \mathbf{g}(\mathbf{x}) + \mathbf{w}$, where $\mathbf{w} \in \mathbb{R}^N$ is a random vector zero-mean Gaussian with covariance matrix $\mathbf{C}$, the likelihood function of $\mathbf{x}$ is given as [34]

$$f_{\widehat{\mathbf{z}}}(\widehat{\mathbf{z}}; \mathbf{x}) = \frac{1}{|2\pi\mathbf{C}|^{\frac{1}{2}}} \exp\left\{ -\frac{1}{2} (\widehat{\mathbf{z}} - \mathbf{g}(\mathbf{x}))^T \mathbf{C}^{-1} (\widehat{\mathbf{z}} - \mathbf{g}(\mathbf{x})) \right\} \tag{9}$$

For an unbiased estimate $\widehat{\mathbf{x}}$ of $\mathbf{x}$, the CRB matrix gives the lowest bound for error covariance matrix among any unbiased estimators [34]. That is

$$E\{(\widehat{\mathbf{x}} - \mathbf{x})(\widehat{\mathbf{x}} - \mathbf{x})^T\} \geqslant \text{CRB}(\mathbf{x}) \stackrel{\Delta}{=} \boldsymbol{\Phi}(\mathbf{x})^{-1}. \tag{10}$$

Here, $\boldsymbol{\Phi}(\mathbf{x})$ is the Fisher information matrix which is the inverse of CRB matrix and its (i, j)th entry is [34],

$$\begin{aligned} [\boldsymbol{\Phi}(\mathbf{x})]_{i,j} &= E\left[\frac{\partial}{\partial x_i} \ln(f_{\widehat{\mathbf{z}}}(\widehat{\mathbf{z}}; \mathbf{x})) \frac{\partial}{\partial x_j} \ln(f_{\widehat{\mathbf{z}}}(\widehat{\mathbf{z}}; \mathbf{x})) \right] \\ &= \frac{\partial \mathbf{g}^T}{\partial \mathbf{x}_i} \boldsymbol{\Sigma}^{-1} \frac{\partial \mathbf{g}}{\partial \mathbf{x}_j} + \frac{1}{2} \mathbf{Tr}\left(\boldsymbol{\Sigma}^{-1} \frac{\partial \boldsymbol{\Sigma}}{\partial \mathbf{x}_i} \boldsymbol{\Sigma}^{-1} \frac{\partial \boldsymbol{\Sigma}}{\partial \mathbf{x}_j} \right). \end{aligned} \tag{11}$$

In the case that the noise covariance matrix $\mathbf{C}$ is independent of $\mathbf{x}$, we obtain

$$\boldsymbol{\Phi}(\mathbf{x}) = (\nabla_{\mathbf{x}} \mathbf{g}(\mathbf{x}))^T \mathbf{C}^{-1} (\nabla_{\mathbf{x}} \mathbf{g}(\mathbf{x})), \tag{12}$$

In the above equation, $\nabla_{\mathbf{x}} \mathbf{g}(\mathbf{x})$ is the Jacobian of $\mathbf{g}(\mathbf{x})$. Based on (12), we obtain the FIM for RSSD localization problem as follows

$$\boldsymbol{\Phi} = \begin{bmatrix} \boldsymbol{\Phi}_{11} & \boldsymbol{\Phi}_{12} \\ \boldsymbol{\Phi}_{21} & \boldsymbol{\Phi}_{22} \end{bmatrix} = (\nabla_{\mathbf{p}} \boldsymbol{\Delta})^T \boldsymbol{\Sigma}^{-1} (\nabla_{\mathbf{p}} \boldsymbol{\Delta}) = \mathbf{J}^T \boldsymbol{\Sigma}^{-1} \mathbf{J}, \tag{13}$$

in which $\mathbf{J} \stackrel{\Delta}{=} (\mathbf{V}_{\mathbf{p}} \boldsymbol{\Delta})$ is the $(N-1) \times 2$ Jacobian matrix which is computed as follows

$$\mathbf{J} = \left[\frac{\partial(\boldsymbol{\Delta})}{\partial \mathbf{x}} \; \frac{\partial(\boldsymbol{\Delta})}{\partial y} \right]^T = \begin{bmatrix} (\mathbf{z}_1 - \mathbf{z}_N)^T \\ \vdots \\ (\mathbf{z}_{N-1} - \mathbf{z}_N)^T \end{bmatrix}, \tag{14}$$

in the above relation $\mathbf{z}_i = \frac{\beta}{r_i} [\cos\theta_i \quad \sin\theta_i]^T$ and $\beta = \frac{10\gamma}{\ln 10}$.

Putting back (14) into (13) and useing $\boldsymbol{\Sigma}^{-1}$ as computed in Appendix-A, with some mathematical manipulations we obtain

$$\boldsymbol{\Phi} = \sum_{i=1}^{N} \frac{1}{\sigma_i^2} \mathbf{z}_i \mathbf{z}_i^T - \alpha \left(\sum_{i=1}^{N} \frac{1}{\sigma_i^2} \mathbf{z}_i \right) \left(\sum_{i=1}^{N} \frac{1}{\sigma_i^2} \mathbf{z}_i \right)^T. \tag{15}$$

where $\alpha = \left(\sum_{i=1}^{N} \frac{1}{\sigma_i^2} \right)^{-1}$. Now, we substitute $\mathbf{z}_i$ into (15) to obtain the entries of symmetric FIM as

$$\boldsymbol{\Phi}_{11} = \beta^2 \left[\sum_{i=1}^{N} \frac{\cos^2\theta_i}{r_i^2 \sigma_i^2} - \alpha \left(\sum_{i=1}^{N} \frac{\cos\theta_i}{r_i^2 \sigma_i^2} \right)^2 \right], \tag{16a}$$

$$\boldsymbol{\Phi}_{12} = \boldsymbol{\Phi}_{21} = \beta^2 \left[\frac{1}{2} \sum_{i=1}^{N} \frac{\sin 2\theta_i}{r_i^2 \sigma_i^2} - \alpha \sum_{i=1}^{N} \frac{\cos\theta_i}{r_i \sigma_i^2} \sum_{i=1}^{N} \frac{\sin\theta_i}{r_i \sigma_i^2} \right], \tag{16b}$$

$$\boldsymbol{\Phi}_{22} = \beta^2 \left[\sum_{i=1}^{N} \frac{\sin^2\theta_i}{r_i^2 \sigma_i^2} - \alpha \left(\sum_{i=1}^{N} \frac{\sin\theta_i}{r_i^2 \sigma_i^2} \right)^2 \right], \tag{16c}$$

The Cramer-Rao lower bound (CRLB) is computed as

$$\text{CRLB} = \sqrt{\frac{\boldsymbol{\Phi}_{11} + \boldsymbol{\Phi}_{22}}{|\boldsymbol{\Phi}|}}. \tag{17}$$

4 Optimum sensors arrangement

To analyze the relative sensor-source geometry we use the determinant of Fisher information matrix as our cost function. In the sequel, we obtain the relative sensor source geometries which maximize the determinant of FIM.

4.1 Determinant of FIM

The determinant of FIM in (16) can be written as

$$|\boldsymbol{\Phi}|=\frac{\beta^4}{4}\left[\left(\sum_{i=1}^{N}\frac{1}{r_i^2\sigma_i^2}\right)^2-\left(\sum_{i=1}^{N}\frac{\cos 2\theta_i}{r_i^2\sigma_i^2}\right)^2-\left(\sum_{i=1}^{N}\frac{\sin 2\theta_i}{r_i^2\sigma_i^2}\right)^2\right]$$
$$-\alpha\beta^4\left[\sum_{i=1}^{N}\frac{\cos^2\theta_i}{r_i^2\sigma_i^2}\left(\sum_{i=1}^{N}\frac{\sin\theta_i}{r_i\sigma_i^2}\right)^2+\sum_{i=1}^{N}\frac{\sin^2\theta_i}{r_i^2\sigma_i^2}\left(\sum_{i=1}^{N}\frac{\cos\theta_i}{r_i\sigma_i^2}\right)\right.$$
$$\left.-\sum_{i=1}^{N}\frac{\sin 2\theta_i}{r_i^2\sigma_i^2}\left(\sum_{i=1}^{N}\frac{\cos\theta_i}{r_i\sigma_i^2}\right)\left(\sum_{i=1}^{N}\frac{\sin\theta_i}{r_i\sigma_i^2}\right)\right]. \tag{18}$$

It can be seen that the determinant of the Fisher information matrix depends on range vector $\mathbf{r}\triangleq[r_1\ \cdots\ r_N]^T$ and observation angle vector $\boldsymbol{\theta}\triangleq[\theta_i\ \cdots\ \theta_N]^T$.

Theorem 1 *For arbitrary SSG when* $\{r_i\}_{i=1}^N$ *and* $\{\sigma_i\}_{i=1}^N$ *are known fixed, the maximization of the determinant of FIM over* $\boldsymbol{\theta}$ *is equivalent to following optimization problem*

$$\widehat{\boldsymbol{\theta}}=\arg\ \min_{\boldsymbol{\theta}}\left\|\sum_{i=1}^{N}\frac{\mathbf{v}(\theta_i)}{r_i^2\sigma_i^2}\right\|_2^2+4\alpha\left\|\sum_{i=1}^{N}\frac{\mathbf{u}(\theta_i)}{r_i\sigma_i^2}\right\|_{\mathbf{H}}^2 \tag{19}$$

in which $\mathbf{u}(\theta_i)=[\cos\theta_i\ \ \sin\theta_i]^T$, $\mathbf{v}(\theta_i)=[\cos 2\theta_i\ \ \sin 2\theta_i]^T$ *and* $\mathbf{H}=\sum_{j=1}^{N}\frac{1}{r_j^2\sigma_j^2}\mathbf{u}(\theta_j-\frac{\pi}{2})\ \ \mathbf{u}^T(\theta_j-\frac{\pi}{2})$ *which is positive definite matrix unless* θ_j *are equal.*

Proof We rewrite the $|\boldsymbol{\Phi}|$ in (18) as

$$|\Phi|=\frac{\beta^4}{4}\left(\sum_{i=1}^{N}\frac{1}{r_i^2\sigma_i^2}\right)^2-\frac{\beta^4}{4}\left[\left(\sum_{i=1}^{N}\frac{\cos 2\theta_i}{r_i^2\sigma_i^2}\right)^2+\left(\sum_{i=1}^{N}\frac{\sin 2\theta_i}{r_i^2\sigma_i^2}\right)^2\right.$$
$$\left.+4\,\alpha\sum_{i=1}^{N}\frac{1}{r_i^2\sigma_i^2}\left(\sin\theta_i\sum_{j=1}^{N}\frac{\cos\theta_i}{r_j\sigma_j^2}-\cos\theta_i\sum_{j=1}^{N}\frac{\sin\theta_i}{r_j\sigma_j^2}\right)^2\right]. \tag{20}$$

Since $|\boldsymbol{\Phi}|\geqslant 0$ and the first term in the right hand of above equation is positive, clearly to maximize $|\boldsymbol{\Phi}|$ over $\boldsymbol{\theta}$, it is sufficient to minimize the terms in the bracket in above equation over $\boldsymbol{\theta}$ as

$$\arg\ \max_{\boldsymbol{\theta}}|\boldsymbol{\Phi}|\equiv\arg\ \min_{\boldsymbol{\theta}}J(\mathbf{r},\boldsymbol{\theta}), \tag{21}$$

where

$$J(\mathbf{r},\boldsymbol{\theta})\triangleq\left(\sum_{i=1}^{N}\frac{\cos 2\theta_i}{r_i^2\sigma_i^2}\right)^2+\left(\sum_{i=1}^{N}\frac{\sin 2\theta_i}{r_i^2\sigma_i^2}\right)^2$$
$$+4\alpha\sum_{i=1}^{N}\frac{1}{r_i^2\sigma_i^2}\left(\cos\theta_i\sum_{j=1}^{N}\frac{\sin\theta_j}{r_j\sigma_j^2}-\sin\theta_i\sum_{j=1}^{N}\frac{\cos\theta_j}{r_j\sigma_j^2}\right)^2. \tag{22}$$

the above relation can be re-written as

$$J(\mathbf{r},\boldsymbol{\theta})=\left\|\sum_{i=1}^{N}\frac{\mathbf{v}(\theta_i)}{r_i^2\sigma_i^2}\right\|^2+4\alpha\left[\sum_{i=1}^{N}\frac{\cos\theta_i}{r_i\sigma_i^2}\ \ \sum_{i=1}^{N}\frac{\sin\theta_i}{r_i\sigma_i^2}\right]\mathbf{H}\begin{bmatrix}\sum_{i=1}^{N}\frac{\cos\theta_i}{r_i\sigma_i^2}\\ \sum_{i=1}^{N}\frac{\sin\theta_i}{r_i\sigma_i^2}\end{bmatrix}$$
$$=\left\|\sum_{i=1}^{N}\frac{\mathbf{v}(\theta_i)}{r_i^2\sigma_i^2}\right\|^2+4\alpha\left\|\sum_{i=1}^{N}\frac{\mathbf{u}(\theta_i)}{r_i\sigma_i^2}\right\|_{\mathbf{H}}^2. \tag{23}$$

□

4.2 Optimal SSG for some special scenarios

In this subsection we study the optimal sensor placement for various scenarios.

Theorem 2 *In the case where the distances* $\{r_i\}_{i=1}^N$ *are known fixed, the maximum attainable value of determinant of FIM is* $|\boldsymbol{\Phi}|_{\max}=\frac{\beta^4}{4}\left(\sum_{i=1}^{N}\frac{1}{r_i^2\sigma_i^2}\right)^2$ *which is obtained if and only if the following two equalities holds.*

$$\sum_{i=1}^{N}\frac{\mathbf{v}(\theta_i)}{r_i^2\sigma_i^2}=0, \tag{24a}$$

$$\sum_{i=1}^{N}\frac{\mathbf{u}(\theta_i)}{r_i\sigma_i^2}=0. \tag{24b}$$

Proof From (18) and (22) we can write

$$|\boldsymbol{\Phi}|=\frac{\beta^4}{4}\left[\left(\sum_{i=1}^{N}\frac{1}{r_i^2\sigma_i^2}\right)^2-J(\mathbf{r},\boldsymbol{\theta})\right]\leqslant\frac{\beta^4}{4}\left(\sum_{i=1}^{N}\frac{1}{r_i^2\sigma_i^2}\right)^2 \tag{25}$$

it is easy to see that the maximum of $|\boldsymbol{\Phi}|$ is obtained whenever the two norms in (23) are zero, hence the optimal conditions (24) are obtained. ■

In this paper the geometries which satisfy these conditions are called as the optimal geometries. On the other hand the geometries which cannot satisfy the conditions Eqs (24), but $|\boldsymbol{\Phi}|$ is maximized with the proper adjustment of $\{\theta_i\}_{i=1}^N$, are called as the sub-optimal geometries. It is easy the following corollary from the conclude of theorem-2.

Corollary 1 *For equal sensor-source ranges (i.e., when* $r_1=\cdots=r_N=r$*), and equal noise variances* $\sigma_1=\cdots=\sigma_N=\sigma$*, the upper bound of determinant of FIM is*

$$|\boldsymbol{\Phi}|\leqslant\frac{\beta^4N^2}{4r^4\sigma^4}. \tag{26}$$

where the equality holds if and only if

$$\sum_{i=1}^{N} \mathbf{u}(\theta_i) = 0, \tag{27a}$$

$$\sum_{i=1}^{N} \mathbf{v}(\theta_i) = 0, \tag{27b}$$

and in this scenario we have

$$\mathrm{CRLB} = \frac{2r\sigma}{\beta\sqrt{N}}. \tag{28}$$

□

Corollary 2 *For $N \geqslant 3$ with the equal sensor-source ranges $r_1 = \cdots = r_N = r$ and equal noise variances $\sigma_1 = \cdots = \sigma_N = \sigma$, equiangular sensor separation is the optimal geometry.*

Proof By defining the complex number $V \triangleq e^{j\theta_1} + \cdots + e^{j\theta_N}$, we can write

$$\begin{aligned} \sum_{i=1}^{N} \cos\,\theta_i &= |V| \cos \angle V, \\ \sum_{i=1}^{N} \sin\,\theta_i &= |V| \sin \angle V, \end{aligned} \tag{29}$$

where $|\cdot|$ and $\angle$ show the magnitude and the angle of a complex number, respectively. To satisfy the condition (27a), $|v|$ should be zero, which is obtained when $\theta_i s$ have a uniform distribution on $[0, 2\pi]$. Similarly, to satisfy (27b), $2\theta_i s$ should have a uniform distribution on $[0, 4\pi]$.[1] □

Corollary 3 *For $N \geqslant 6$, when the sensor ranges and noise variances are equal, consider that we have partitioned the N sensors into q groups $\{v_1, \ldots, v_q\}$, then an optimal geometry of sensors is obtained if each subset of sensors $\{v_i\}$ satisfies the conditions in (27) regardless of the relative arrangement of individual groups.*

Proof The conditions (27) can be written as

$$\sum_{i=1}^{N} \mathbf{u}(\theta_i) = \sum_{k=1}^{q} \sum_{i \in v_k} \mathbf{u}(\theta_i), \tag{30a}$$

$$\sum_{i=1}^{N} \mathbf{v}(\theta_i) = \sum_{k=1}^{q} \sum_{i \in v_k} \mathbf{v}(\theta_i) \tag{30b}$$

Since for each subset v_i we have $\sum_{i \in v_i} \mathbf{u}(\theta_i) = 0$ and $\sum_{i \in v_i} \mathbf{v}(\theta_i) = 0$, hence the conditions (27) are satisfied. □

[1] We have to mention that for $N \geqslant 6$ with equal sensor ranges, the optimal geometry is not unique and equiangular sensor separation is a special case of infinitely many optimal geometries.

Corollary 4 *For $N = 3$ with the different sensor-source ranges and equal noise variances the determinant of FIM can be obtained as*

$$|\boldsymbol{\Phi}| = \frac{\beta^4}{3\sigma^4 (r_1 r_2 r_3)^2} \left[r_3 \sin(A) - r_2 \sin(B) - r_1 \sin(A - B) \right]^2 \tag{31}$$

in which, $A = \theta_2 - \theta_1, B = \theta_3 - \theta_1$.

To obtain the optimal angular sensor separation, by taking the partial derivative of $|\boldsymbol{\Phi}|$ with respect to A and B, optimal geometry can be obtained when either

$$r_3 \cos(A) = r_2 \cos(B) = r_1 \cos(A - B) \tag{32}$$

or

$$r_3 \sin(A) = r_2 \sin(B) + r_1 \sin(A - B) \tag{33}$$

□

To obtain optimal sensor placement for different sensor-source ranges using the gradient of FIM determinant, we can update the sensor configuration, so as to yield an increase in the specified convex combination of the FIM determinant.

5 Computer simulations

In this section, first, we present simulation results for two scenarios with equal sensor ranges and different sensor ranges. Then, we compare the performance of purposed optimal sensor placemnt for N=3,6 with other placements. Furthermore we present optimal placement based on the A-optimality and D-optimality. Finally we study the effect of sensor ranges on optimal sensor placement. In our simulation we assume $\gamma = 2, (\sigma_1 = \sigma_2 = \ldots = \sigma_N = -20\mathrm{dB})$ and we consider the sensor with angle $\theta_1 = 0^\circ$ as the reference.

5.1 Equal sensor ranges

At first, we study optimal sensor geometries for $N = 3, 4$ with the equal sensor ranges $(r_i = 1000\,\mathrm{m}, i = 1, 2, 3, 4)$. Figure 2 presents the determinant of FIM and the corresponding contour plot versus θ_2 and θ_3 for $N = 3$ with the equal sensor ranges. As Fig. 2b shows, the maximum value of $|\boldsymbol{\Phi}|$ is attained when $\theta_2 = 120^\circ$, $\theta_3 = 240^\circ$ which validate the Corollary 1. Since the maximum value of $|\boldsymbol{\Phi}|$ is 1.2807, which is equal to the upper-bound of Corollary 1, this solution is optimal geometry.

Figure 3 shows the $|\boldsymbol{\Phi}|$ as function of θ_3 and θ_4 for $N = 4$, $\theta_1 = 0^\circ, \theta_2 = 90^\circ$ with the equal sensor ranges.

Similar to the above example, equiangular sensor separation (i.e., $\theta_3 = 180^\circ, \theta_4 = 270^\circ$) gives the optimal

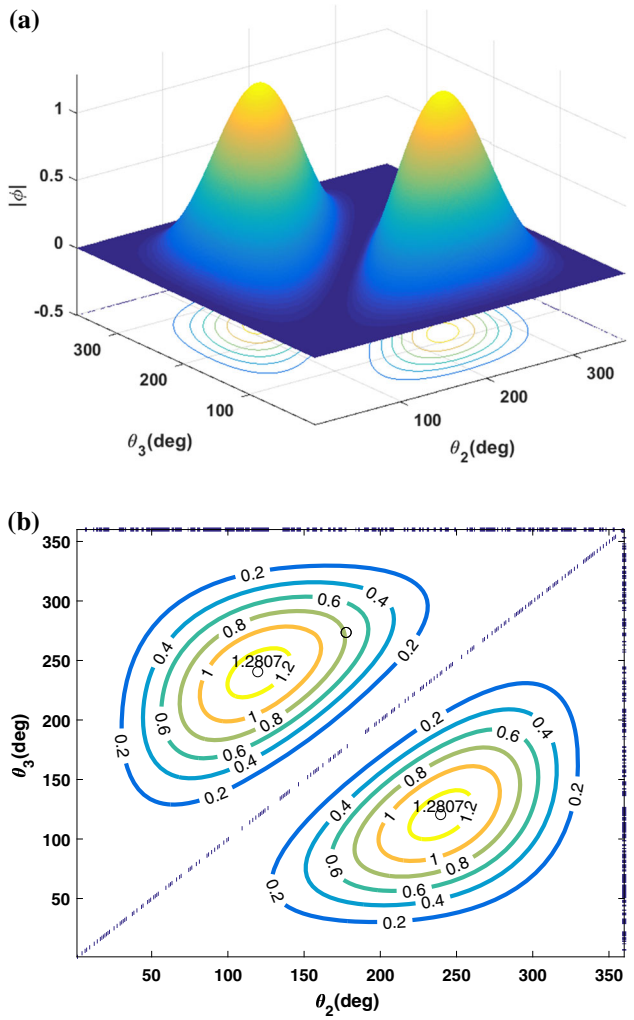

Fig. 2 **a** Determinant of FIM as a function of θ_2 and θ_3 for $N = 3$ with the equal sensor ranges; **b** contour plot of the determinant of FIM

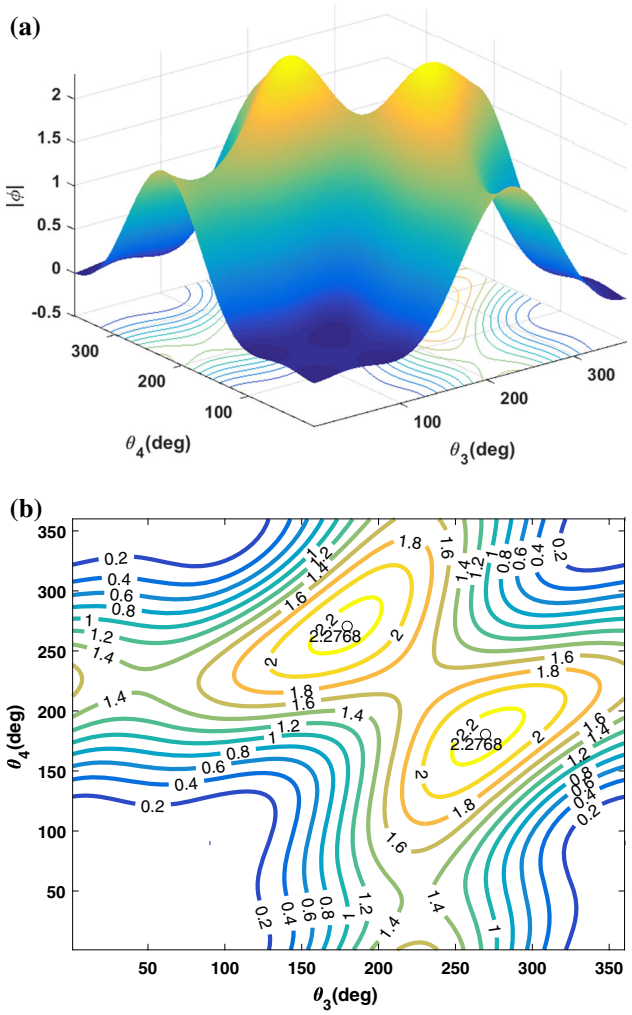

Fig. 3 **a** Determinant of FIM as a function of θ_3 and θ_4 for $N = 4$, $\theta_2 = 90^\circ$ with equal sensor ranges; **b** the contour plot of the determinant of FIM

sensor geometry where $|\boldsymbol{\Phi}| = 2.2768$. Two optimal geometries for $N = 3,\ 4$ are illustrated in Fig. 4.

5.2 Different sensor ranges

Here, we study SSG when the sensors are located at different distances to the source. At first, we consider $N = 3$ and $(r_1, r_2, r_3) = (1000\,\text{m}, 1000\,\text{m}, 800\,\text{m})$. Figure 5, shows the determinant and contour plot of FIM versus θ_2 and θ_3. As Fig. 5b shows the maximum value of $|\boldsymbol{\Phi}|$ is 1.7495, which is attained whenever

$$\{(\theta_2, \theta_3)\} \in \{(125^\circ,\ 242^\circ), (235^\circ,\ 118^\circ)\}.$$

Since this maximum cannot reach to the upper bound of Theorem-2 (i.e., 1.806), these solutions are sub-optimal geometries. Two distinct sub-optimal geometries are illustrated in Fig. 6.

The determinant of FIM and corresponding contour plot versus θ_3 and θ_4 for $N = 4$ are illustrated in Fig. 7.

The bearing angle pairs $\{(\theta_3, \theta_4)\}$ which maximize the determinant of FIM are given by the set of $\{(\theta_3, \theta_4)\} \in \{(178^\circ, 273^\circ), (280^\circ, 185^\circ)\}$. Here, the maximum value of $|\boldsymbol{\Phi}|$ cannot reach to the upper bound of Theorem 2 (i.e.,4.8496), which two distinct sub-optimal configurations are illustrated in Fig. 8.

5.3 Comparison of different sensor placements

In this part, we consider a region 1000 m $\times$ 1000 m where the sensors are located at the stationary positions on the circle around the origin $[0, 0]^T$ with radios 1000 m, then we plot the FIM determinant in this region. To study the performance of different of sensor placements, we compute two criteria including, the average $|\boldsymbol{\Phi}|$ as $\text{AV}_{|\boldsymbol{\Phi}|}$ and the $|\boldsymbol{\Phi}|$

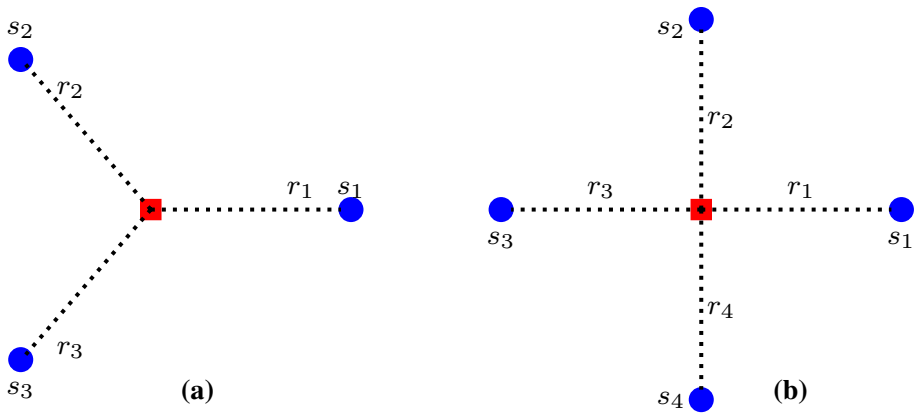

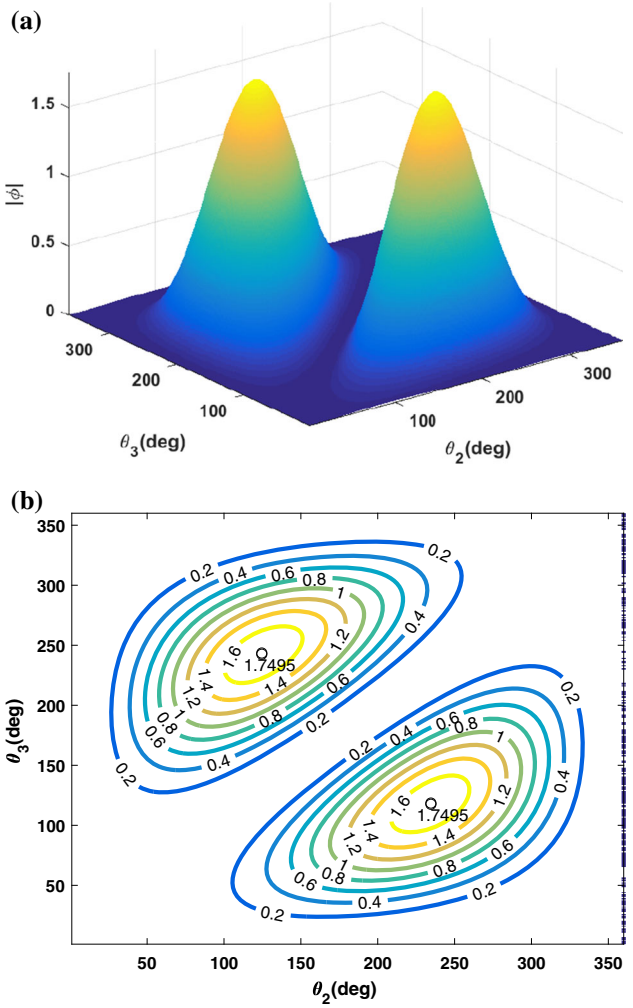

Fig. 4 **a** Optimal SSG for $N = 3$; **b** optimal SSG for $N = 4$

Fig. 5 **a** Determinant of FIM as a function of θ_2 and θ_3 for $N = 3$ with $(r_1, r_2, r_3) = (1000\text{m}, 1000\text{m}, 800\text{m})$; **b** contour plot of the determinant of FIM

at the origin as $|\boldsymbol{\Phi}|_{(0,0)}$. We know the higher level of $|\boldsymbol{\Phi}|$ or $\text{AV}_{|\boldsymbol{\Phi}|}$ give a batter performance.

Figure 9a shows the $|\boldsymbol{\Phi}|$ for $N = 3$ with equiangular sensor separation 120°. Figure 9b shows the $|\boldsymbol{\Phi}|$ for $\theta_1 = 0°, \theta_2 = 60°, \theta_3 = 120°$. By Comparing two placements, equiangular sensor separation gives a better performance due to the higher $\text{AV}_{|\boldsymbol{\Phi}|}$ and higher $|\boldsymbol{\Phi}|_{(0,0)}$, which validates the Corollary 1.[2]

Figure 10 shows $|\boldsymbol{\Phi}|$ for two placements with $N = 6$ sensors. As Fig. 10 illustrates, the first placement with equiangular sensor separation 60° gives a better performance in average due to higher $\text{AV}_{|\boldsymbol{\Phi}|}$. On the other hand when the source is located at the origin, the two placements give equal performance due to equal $|\boldsymbol{\Phi}|_{(0,0)}$ which validates the Corollary 1, because in the second placement, the sensors are partitioned into two sets $\{s_1, s_2, s_3\}$ and $\{s_4, s_5, s_6\}$ with equiangular sensor separation 120°.

5.4 Optimal placement based on D-optimality and A-optimality

Here we consider two criteria for optimal sensor placement including maximization of determinant of FIM (D-optimality), and minimization of the trace of the inverse of FIM (A-optimality). D-optimality criterion minimizes the volume of the uncertainty ellipsoid for the source estimation [27]. A-optimality criterion, which consists in minimizing the trace of the CRLB matrix, suppresses the average variance of the estimation error, this creation introduced in Eq. (17). Now, we consider three sensors such that the source is located at the origin $[0, 0]^T$. Figure 11(a) shows the plot of CRLB as a function of θ_{21} and θ_{31}. The optimal angels which minimizing CRLB are either $(\theta_{21}, \theta_{31}) = (128°, 244°)$ or $(\theta_{21}, \theta_{31}) = (230°, 116°)$. In Fig. 11(b), the plot of $|\boldsymbol{\Phi}|$ is provided. The optimal angle that maximizing $|\boldsymbol{\Phi}|$ are either $(\theta_{21}, \theta_{31}) = (125°, 243°)$ or

[2] Although some places in the Fig. 9b have better performance respect to the corresponding places in Fig. 9a but in average the sensor configuration in Fig. 9a gives a better performance for all region.

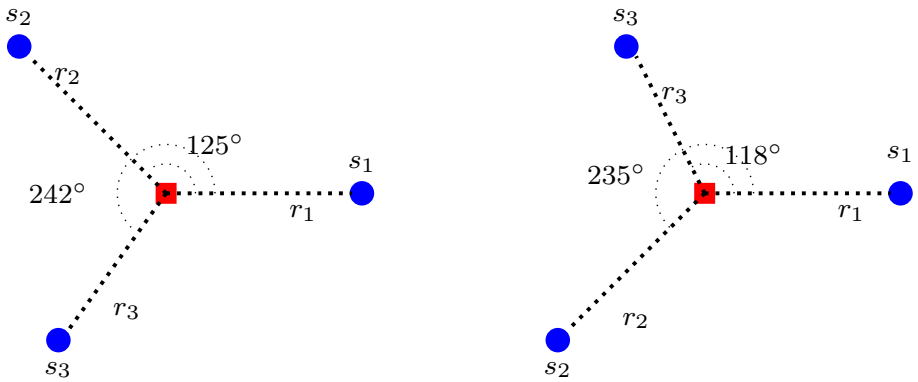

Fig. 6 Two sub-optimal SSG for $N = 3$ and $(r_1, r_2, r_3) = (1000, 1000, 800)$m

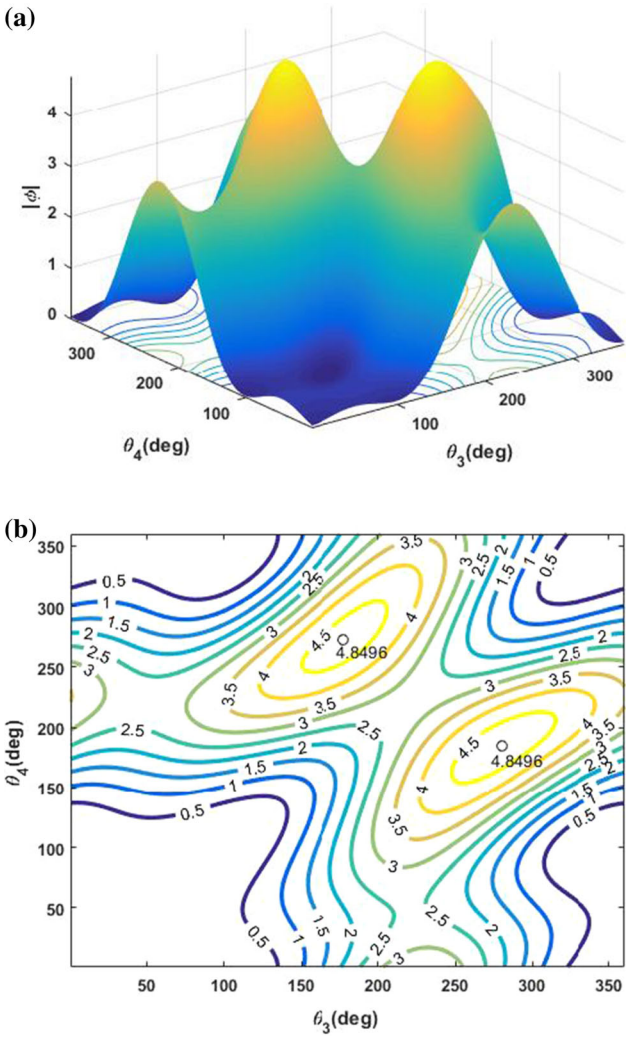

Fig. 7 **a** The determinant of FIM as a function of θ_3 and θ_4 for $N = 4$, $\theta_2 = 90°$ and $(r_1, r_2, r_3, r_4) = (1000\text{m}, 900\text{m}, 800\text{m}, 700\text{m})$; **b** The contour plot of the determinant of FIM

$(\theta_{21}, \theta_{31}) = (235°, 118°)$. We observe that D-optimality and A-optimality, yield different sensor placements, whereas it has been shown in AOA-optimization geometry, the A-optimality is equivalent to the D-optimality [27].

5.5 Effect of sensor ranges on the performance of optimal placement

We study the effect of sensor ranges on the performance of optimal geometry using determinant of FIM. Based on previous statement, we know the higher level of $|\boldsymbol{\Phi}|$ gives the better performance because it leads to minimization of uncertainty ellipsoid. We consider optimal geometries for $N = 3, 4, 5$, where the source is located at the center of these sensors. Then we plot the CRLB curves versus different sensor ranges in Fig. 12. As can be seen, with increasing the sensor ranges the $|\boldsymbol{\Phi}|$ will be minimized. This means that with increasing the sensor ranges the uncertainty area of the source estimation will be maximized.

6 Conclusion

In this paper, we provided a characterization of optimal sensor placement for RSSD based source localization using the maximization of determinant of FIM. We derived the necessary and sufficient conditions to obtain the optimal sensor placement for different scenarios. The results of this paper can be used to place the sensors around the source in order to obtain the best performance for source localization. Simulation results showed that the optimal sensor placement has a good performance compared to the other placements. Future work can focus on extending the results

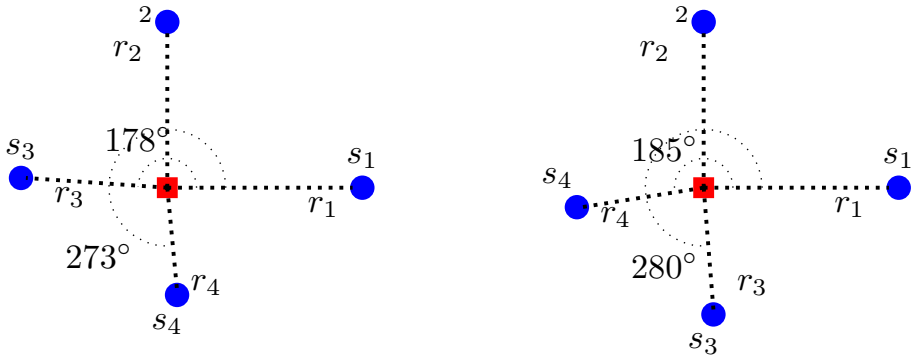

Fig. 8 Two sub-optimal SSG for $N = 4$ and $(r_1, r_2, r_3, r_4) = (1000, 900, 800, 700)$m

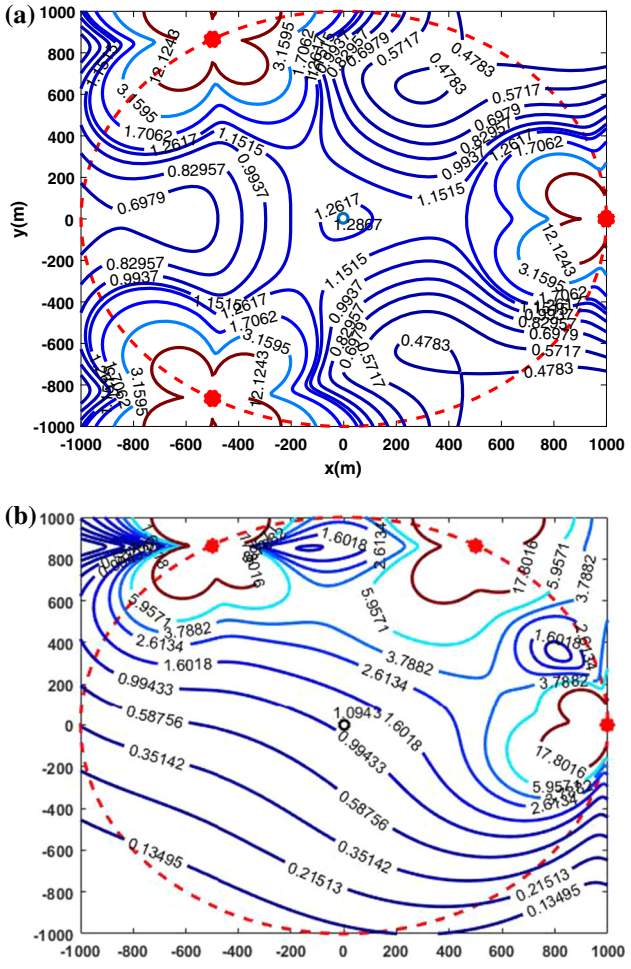

Fig. 9 **a** The contour plot of the determinant of FIM for $N = 3$ with $\theta_1 = 0°, \theta_2 = 120°, \theta_3 = 240°$, $\text{AV}_{|\boldsymbol{\Phi}|} = 1595$ and $|\boldsymbol{\Phi}|_{(0,0)} = 1.2867$; **b** the contour plot of the determinant of FIM for $N = 3$ with $\theta_1 = 0°, \theta_2 = 60°, \theta_3 = 120°$, $\text{AV}_{|\boldsymbol{\Phi}|} = 1576$ and $|\boldsymbol{\Phi}|_{(0,0)} = 1.0943$

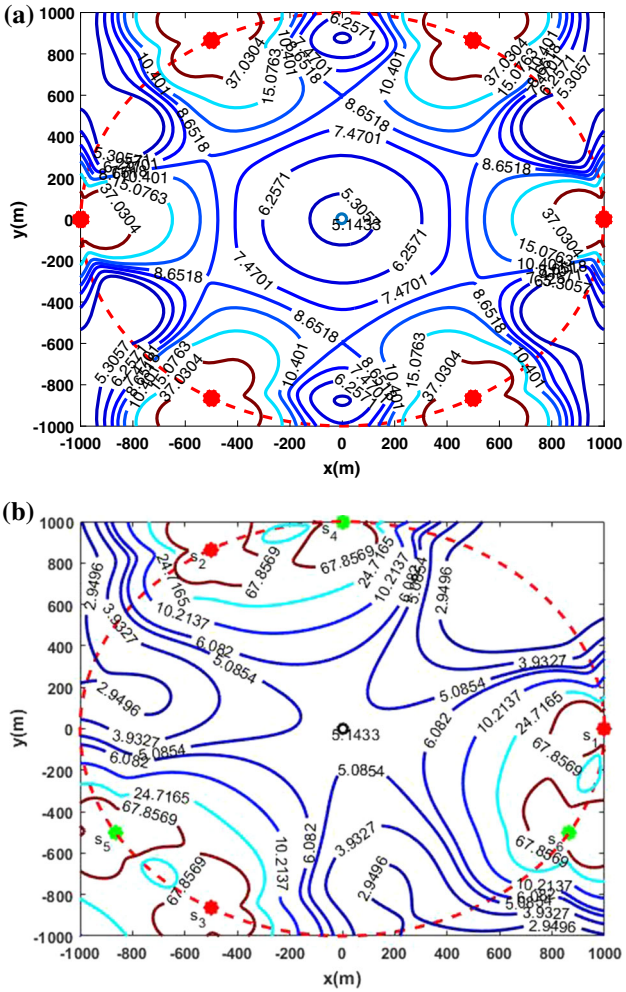

Fig. 10 **a** The contour plot of the determinant of FIM for $N = 6$ with equiangular sensor sepearation 60°, $\text{AV}_{|\boldsymbol{\Phi}|} = 1895$ and $|\boldsymbol{\Phi}|_{(0,0)} = 5.1433$; **b** the contour plot of the determinant of FIM for $\{\theta_1 = 0°, \theta_2 = 120°, \theta_3 = 240°\}, \{\theta_4 = 90°, \theta_4 = 210°, \theta_4 = 330°\}$, $\text{AV}_{|\boldsymbol{\Phi}|} = 1819$ and $|\boldsymbol{\Phi}|_{(0,0)} = 5.1433$

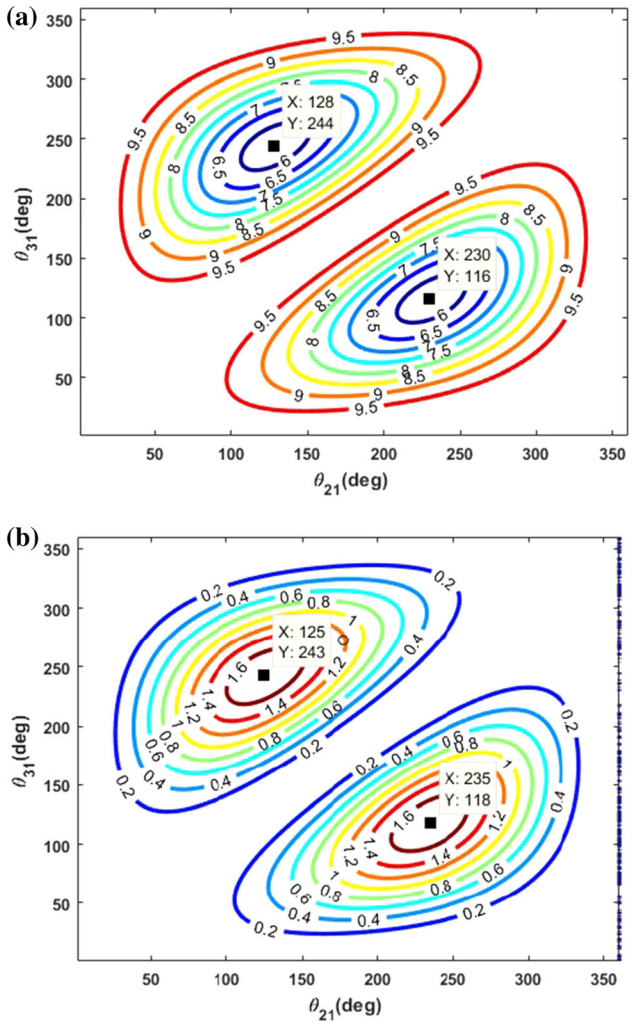

Fig. 11 **a** Contour plot of CRLB with $(r_1, r_2, r_3) = (1000, 1000, 800)$ m; **b** contour plot of determinant of FIM

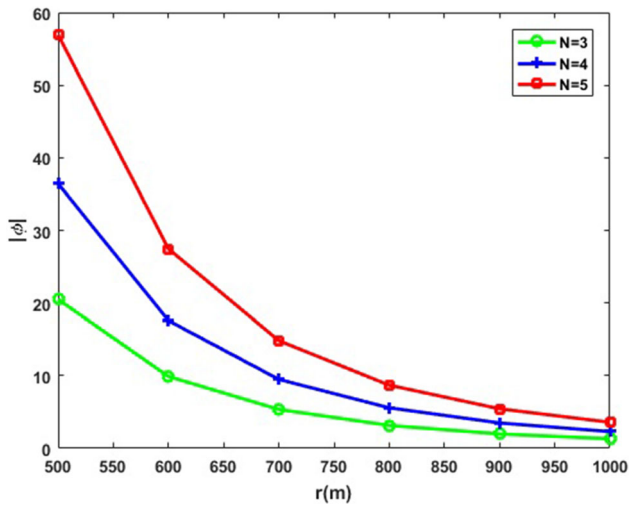

Fig. 12 Determinant of FIM versus sensor ranges

of this paper to optimal trajectory control for moving RSSD sensor platforms and the optimal sensor geometries for heterogeneous sensor networks.

Appendix A

Using the matrix inversion lemma [35]

$$(\mathbf{A}+\mathbf{BCD})^{-1} = \mathbf{A}^{-1} - \mathbf{A}^{-1}\mathbf{B}\left(\mathbf{C}^{-1}+\mathbf{DA}^{-1}\mathbf{B}\right)^{-1}\mathbf{DA}^{-1}, \tag{34}$$

where

$$\mathbf{A} = \text{diag}\left[\sigma_1^2, ..., \sigma_{N-1}^2\right], \mathbf{B} = \left[1 \quad ... \quad 1\right]^T, \mathbf{C} = \sigma_N^2, \text{ and } \mathbf{D} = \mathbf{B}^T$$

Hence the inverse of $\boldsymbol{\Sigma}$ in Eq (8) can be written as

$$\boldsymbol{\Sigma}^{-1} = \mathbf{A}^{-1} - \alpha \mathbf{s}\mathbf{s}^T, \tag{35}$$

where $\alpha = \left(\sum_{i=1}^{N} \frac{1}{\sigma_i^2}\right)^{-1}$ and $\mathbf{s} = \left[\frac{1}{\sigma_1^2} \quad ... \quad \frac{1}{\sigma_{N-1}^2}\right]^T$.

References

1. Wang, Y., & Ho, K. C. (2015). An symptotically efficient estimator in closed-form for 3-D AOA localization using a sensor network. *IEEE Transactions on Wireless Communnications*, *14*(12), 6524–6535.
2. Miao, Q., & Huang, B. (2018). On the optimal anchor placement in single-hop sensor localization. *Wireless Networks*, *24*(5), 1609–1620.
3. Lohrasbipeydeh, H., Gulliver, T. A., & Amindavar, H. (2014). A minimax SDP method for energy based source localization with unknown transmit power. *IEEE Wireless Communications Letter*, *3*(4), 433–436.
4. Uluskan, S., & Filik, T. (2019). A geometrical closed form solution for RSS based far-field localization: Direction of Exponent Uncertainty. *Wireless Networks*, *25*(1), 215–227.
5. Jin, R., Che, Z., Xu, H., Wang, Z., & Wang, L. (2015). An RSSI-based localization algorithm for outliers suppression in wireless sensor networks. *Wireless Networks.*, *21*(8), 2561–2569.
6. Liu, D., Lee, M., Pun, C., & Liu H (2013) Analysis of wireless localization in nonline-of-sight conditions. *IEEE Transactions on Vehicular Technology, 62*(4), 1484-1492. Networking Conference, WCNC, 1–6.
7. Catovic, A., & Sahinoglu, Z. (2004). The cramer-rao bounds of hybrid TOA/RSS and TDOA/RSS location estimation schemes. *IEEE Communications Letters*, *8*(10), 626–628.
8. Park, C. H., & Chang, J. H. (2017). TOA source localization and DOA estimation algorithms using prior distribution for calibrated source. *Digital Signal Processing*, *71*, 61–68.
9. Wang, J., Chen, J., & Cabric, D. (2013). Cramer-rao bounds for joint RSS/DoA-based primary-user localization in cognitive radio networks. *IEEE Transactions on Wireless Communications*, *12*(3), 1363–1375.
10. Ma, W. K., Vo, B. N., Singh, S. S., & Baddeley, A. (2006). Tracking an unknown time-varying number of speakers using TDOA measurements: A random finite set approach. *IEEE Transactions on Signal Processing*, *54*(9), 3291–3303.

11. Meesookho, C., Mitra, U., & Narayanan, S. (2008). On energy-based acoustic source localization for sensor networks. *IEEE Transactions on Signal Processing*, *56*(1), 365–377.
12. Thompson, A. R., Moran, J. M., & Swenson, G. W. (2008). *Interferometry and Synthesis in Radio Astronomy*. New York: Wiley.
13. Biguesh, M. (2016). Bearing estimation using time delays: optimum sensor arrangement and an efficient estimator. *IEEE Sensor Journal*, *16*(18), 6961–6965.
14. Shen, J., Molisch, A. F., & Salmi, J. (2012). Accurate passive location estimation using TOA measurements. *IEEE Transactions on Wireless Communications*, *11*(6), 2182–2192.
15. Wu, N., Yuan, W., Wang, H., & Kuang, J. (2016). TOA-based passive localization of multiple targets with inaccurate receivers based on belief propagation on factor graph. *Digital Signal Processing*, *49*, 14–23.
16. Hurtado, M., & Nehorai, A. (2007). Performance analysis of passive low-grazing-angle source localization in maritime environments using vector sensors. *IEEE Transactions on Aerospace and Electronic Systems*, *43*(2), 780–788.
17. Jean, O., & Weiss, A. J. (2014). Geolocation by direction of arrival using arrays with unknown orientation. *IEEE Transactions on Signal Processing*, *62*(12), 3135–3142.
18. Blatt, D., & Hero, A. O. (2006). Energy-based sensor network source localization via projection onto convex sets. *IEEE Transactions on Signal Processing*, *54*(9), 3614–3619.
19. Klukas, R., & Lachapelle G. (2003). An enhanced two-step least squared approach for TDOA/AOA wireless location. IEEE International Conference on Communications, (ICASSP 03), vol. 2, pp. 987–991.
20. Taponecco, L., Damico, A. A., & Mengali, U. (2011). Joint TOA and AOA estimation for UWB localization applications. *IEEE Transactions on Wireless Communications*, *10*(7), 2207–2217.
21. Biguesh, M., & Gazor, S. (2009). On proper antenna pattern for a simple source detection and localization system. *IEEE Transactions on Antennas and Propagation*, *57*(4), 1073–1080.
22. Liu, B. H., Lin, K. H., & Wu, J. C. (2006). Analysis of hyperbolic and circular positioning algorithms using stationary signal-strength-difference measurements in wireless communications. *IEEE Transactions on vehicular Technology*, *55*(2), 499–509.
23. Patwari, N., Hero, A. O., Perkins, M., Correal, N. S., & Odea, R. J. (2003). Relative location estimation in wireless sensor networks. *IEEE Transactions on Signal Processing*, *51*(8), 2137–2148.
24. Cheung, K. W., So, H. C., Ma, W.-K., & Chan, Y. T. (2003). Received signal strength based mobile positioning via constrained weighted least squares, IEEE International Conference on Acoustics, Speech, and Signal Processing, (ICASSP 03), pp. 137–140.
25. Wang, S., & Inkol, R (2011). A near-optimal least squares solution to received signal strength difference based geolocation. IEEE International Conference on Acoustics, Speech and Signal Processing, (ICASSP 11), pp. 2600–2603.
26. Wang, G., Chen, H., Li, Y., & Jin, M. (2012). On received-signal-strength based localization with unknown transmit power and path loss exponent. *IEEE Wireless Communications Letters*, *1*(5), 536–539.
27. Doganay, K., & Hmam, H. (2008). Optimal angular sensor separation for AOA localization. *Signal Processing*, *88*(5), 1248–1260.
28. Herath., S. C. K, & Pathirana, P. N. (2010). Optimal sensor separation for AoA based localization via linear sensor array. In International Conference on Intelligent Sensors, Sensor Networks and Information Processing, pp. 187–192.
29. Meng, W., Xie, L., & Xiao, W. (2016). Optimal TDOA sensor-pair placement with uncertainty in source location. *IEEE Transactions on Vehicular Technology*, *65*(11), 9260–9271.
30. Lui, K. W. K., & So, H. C. (2009). A study of two-dimensional sensor placement using time-difference-of-arrival measurements. *Digital Signal Processesing*, *19*(4), 650–659.
31. Bishop, A. N., & Jensfelt, P. (2009). An optimality analysis of sensor-target geometries for signal strength based localization. *International Conference on Intelligent Sensors, Sensor Networks and Information Processing*, *1*, 127–132.
32. Meng, W., Xie, L., & Xiao, W. (2013). Optimality analysis of sensor-source geometries in heterogeneous sensor networks. *IEEE Transactions on Wireless Communications*, *12*(4), 1958–1967.
33. Rappaport, T. S. (1999). *Wireless Communications: Principles and Practice*. Englewood Cliffs, NJ, USA: Prentice-Hall.
34. Kay, S. M. (1993). *Fundamentals of Statistical Signal Processing: Estimation Theory*. Upper Saddle River, NJ: Prentice-Hall.
35. Golub, G. H., & van Loan, C. F. (1996). *Matrix Computations*. Baltimore, MD: Johns Hopkins Univ. Press.

Publisher's Note Springer Nature remains neutral with regard to jurisdictional claims in published maps and institutional affiliations.

Ali Heydari was born in Shiraz, Iran. He received the B.Sc. degree in electronics from USB University in 2008 and the M.Sc. degree in communication systems from Shiraz University, Shiraz, Iran in 20011. He is currently Ph.D. candidate at Yazd University, Yazd, Iran. His current research interests are in the area of wireless communications with special emphasis on digital and statistical signal processing, localization, and tracking.

Masoud-Reza Aghabozorgi was born in Yazd, Iran. He received the B.Sc., M.Sc., and Ph.D. degrees from Isfahan University of Technology, Isfahan, Iran, in 1993, 1996, and 2002, respectively, all in electrical engineering. He is currently an Associate Professor with the Department of Electrical Engineering at Yazd University. His main research areas of interest include signal processing, particularly blind source separation, source localization, and wireless communication system.

Mehrzad Biguesh (S'89-M'02-SM'08) received the Ph.D. (Hons.) degree in communication systems from the Sharif University of Technology, Tehran, Iran, in 2000. During 2000 to 2005, he held several full-time and visiting research appointments, in Iran, Germany, and Canada. In 2005, he joined the School of ECE, Shiraz University, where he is a Full Professor. He is the founder and CEO of Esprooz Special Processing (ESP). His research interests include wireless communications, radar signal and data processing, array signal processing, direction estimation, and position finding.